ORIGINAL RESEARCH PAPER

Molecular Dynamics Investigation of The Elastic Constants and Moduli of Single Walled Carbon Nanotubes

Mohammad Mahdi Zaeri *, Saeed Ziaei-Rad

Department of Mechanical Engineering, Isfahan University of Technology, Isfahan, Iran

Received: 2017-04-03 Accepted: 2017-05-16 Published: 2017-06-25

ABSTRACT

Determination of the mechanical properties of carbon nanotubes is an essential step in their applications from macroscopic composites to nano-electro-mechanical systems. In this paper we report the results of a series of molecular dynamics simulations carried out to predict the elastic constants, i.e. the elements of the stiffness tensor, and the elastic moduli, namely the Young's and shear moduli, of various single walled carbon nanotubes. Poisson's ratios were also calculated. Three different methods were used to run the simulations: applying a predetermined strain and reading the resulted stress, applying forces and constraints to the end atoms and calculating the moduli by assuming an equivalent continuum tube, and lastly applying a predetermined stress and reading the consequent deformation. In each case, the effect of nanotube chirality and diameter was studied. In addition, loading conditions were altered in each method to study the effect of nonlinearity of interatomic interactions. The results of the three methods are compared, with each other as well as with the literature, and discussed to obtain reasonable concluding remarks.

Keywords: *Elastic constants; Elastic moduli; Molecular dynamics simulation; Single walled carbon nanotube*

How to cite this article

Zaeri MM, Ziaei-Rad S. Molecular Dynamics Investigation of the Elastic Constants and Moduli of Single Walled Carbon Nanotubes. J. Nanoanalysis., 2017; 4(1): 65-75. DOI: 10.22034/jna.2017.01.008

INTRODUCTION

Carbon nanotubes (CNTs) are the focus of a considerable percent of nanotechnology research. So far many properties of these nanostructures have been investigated either theoretically or experimentally including electrical, electronic, mechanical, chemical, optical and thermal properties. Among these, mechanical properties are of particular importance because numerous studies indicate that they are extraordinarily high in comparison with those of bulk engineering materials such as steels and alloys; see for example the review papers [1-9]. This is promising in many fields, for example fabrication of high strength-to-weight ratio materials applied in aerospace industry, production of new composites, manufacture of excellent thermal conductors, etc. In addition to these practical applications, investigation of the mechanical properties of CNTs is important from the view point of fundamental science as well, because it provides the background for further research and advancement in the outstanding field of nanoscience.

Single walled carbon nanotubes (SWCNTs) are the simplest form of CNTs. An SWCNT can be thought of as a graphene sheet rolled into a hollow cylinder. In perfect structure, it

* Corresponding Author Email: mm.zaeri@me.iut.ac.ir

consists of hexagonal rings in which carbon atoms are placed on the vertices. Depending on the orientation of the rings, it is divided into three types: armchair, zigzag and chiral. Many researchers have devoted their effort to determine the elastic properties of CNTs using different methods such as molecular dynamics (MD), molecular density functional theory, nonlocal elasticity, experimental measurements by atomic force microscope, etc. However, they are mostly focused on the elastic moduli i.e. the axial Young's modulus and the transverse shear modulus, rather than the elastic constants i.e. the elements of the stiffness tensor. The numerous reported results in the literature cover wide ranges of 270-5500 GPa for Young's modulus and 240-2300 GPa for shear modulus [1-32]. There are many reasons, discussed in some original and review papers, why the ranges are so wide. They include dependence on chirality, diameter, number of walls, length and temperature of the CNT, whether it is perfect or defective, whether the study is theoretical or experimental, what theoretical or experimental methods and parameters are used, etc. Nevertheless, from the statistical point of view most of the results are distributed close to a Young's modulus of 1000 GPa or 1 TPa and a shear modulus of 400 GPa, so that these values are well-known and can be used as approximate expected values [1-3,7,8,11-13,18-23,30,32].

Several research groups have developed new methods to study the mechanics of SWCNT such as Zhang et al. who established a continuum theory incorporating interatomic potentials to find the Young's modulus of SWCNT through a constitutive model without any parameter fitting [29]. Based on two sets of interatomic potential parameters they obtained two values of 475 GPa and 705 GPa. Also, Chen and Cao developed a new structural mechanics approach for SWCNTs based on atomistic simulations [33]. In their MD simulations, they used the condensed-phase optimized molecular potential for atomistic simulation studies (COMPASS). Similarly, Chang and Gao presented an analytical model based on molecular mechanics and derived closed-form expressions for Young's modulus and Poisson's ratio of SWCNT as functions of tube diameter [34].

In one of the early MD simulations of SWCNT to predict its mechanical properties, Yao et al. simulated an armchair SWCNT applying the Brenner potential and computed its Young's modulus and tensile strength to be 3.62 TPa and 9.6 GPa respectively [35]. Making a comparison with experimental data (Young's modulus of 0.45 TPa and tensile strength of 3.6 GPa), they suggested that the large difference is due to the structure and size of the SWCNT and the errors of the applied force field. As another early research, Prylutskyy et al. carried out MD simulation of two SWCNT samples [36]. They reported a Young's modulus of about 1.10 TPa and a Poisson's ratio of 0.28.

Jin and Yuan derived some of the effective elastic moduli of armchair SWCNTs through MD simulations using both force and energy approaches [37]. They obtained values close to 1.3 TPa for both the longitudinal and hoop Young's moduli. Also for the longitudinal-hoop plane, values of approximately 0.26 for Poisson's ratio and 0.5 TPa for shear modulus were obtained. Elastic and plastic properties of various CNTs under axial tension were studied using MD by Liew et al. [38]. Applying second-generation reactive empirical bond order (REBO) potential coupled with Lennard-Jones potential, they obtained the stress-strain response and reported values near 1 TPa for the Young's modulus of SWCNT. A Chinese group simulated the elastic response and the buckling modes of SWCNT by MD [39]. They found a range of 1.25-1.48 TPa for Young's modulus. They also found that Young's modulus decreases as the radius of SWCNT increases and that it is higher for zigzag SWCNTs than for armchair ones. Wang et al. ran MD simulations of the twist of CNTs employing the adaptive intermolecular REBO (AIREBO) potential [40]. They did not report any values for the elastic constants but concluded that bigger tubes are harder to be twisted while smaller tubes exhibit higher ultimate twisting ratio.

A comparison between five methods of determination of Young's modulus of SWCNT via MD simulations was made by Agrawal et al. [30]. They consist of (i) determination of stress for a given strain (ii) determination of strain energy (iii) longitudinal vibrations (iv) transverse vibrations and (v) determination of

strain for a given stress. The conclusion is that the result of all methods are consistent (close to 0.75 TPa for an armchair SWCNT) except that of method (iv) which yields lower value (0.55 TPa for the same model). Solutions to solve this problem was suggested by the group. Also it was found that Young's modulus is higher for zigzag tube than armchair tube (~0.85 TPa vs. ~0.75 TPa). An Australian team discussed the important issues in an MD simulation of the mechanical properties of CNTs including selection of appropriate potential, thermostat atoms and techniques, time step, etc. and taking them into account found the Young's modulus and Poisson's ratio for some models [41].

Motevalli et al. performed MD simulations of buckling of SWCNT under simultaneous combination of compressive and torsional loads employing the Tersoff-Brenner potential [42]. In case of pure compression, Young's modulus of 0.76 TPa was obtained. Similarly in case of pure torsion, shear modulus of 0.28 TPa was calculated. Buckling of defective SWCNTs was also investigated with the aid of MD by another team [43]. Among their results an axial Young's modulus of about 1.1 TPa is reported. Effect of Stone-Wales defect on the mechanical properties of SWCNTs was also examined by atomistic simulations [31]. In this study the Young's modulus of perfect samples was close to 0.84 TPa and decreased when the density of defects increased. Finally, Duan et al. studied the fracture of CNT via molecular mechanics using the modified Morse and REBO potentials [44]. They found that with an increase in chiral angle, the tensile strength and fracture strain increase monotonously.

In none of the above mentioned works, one can find a comprehensive analysis of all of the elastic constants (not only the Young's and shear moduli) of various SWCNTs of both armchair and zigzag types obtained through different methods. That is the motivation of this paper. Therefore, in the present work, we aim to determine all of the elastic constants and elastic moduli of various SWCNTs using MD via three methods and compare the results. The first method provides us with the elastic constants, from which Young's and shear moduli as well as Poisson's ratios are further derived. As stated before, elastic constants of SWCNTs are rarely found in the literature. Therefore, this method is of double importance. The second and third methods result directly in the Young's and shear moduli. Overall, the results of these methods provide an insight into the elastic properties of SWCNTs and a basis for comparison with the values in literature obtained through other techniques. In addition, the way applied here for definition of the interatomic interactions (by developing MATLAB codes discussed below) differs from those of previous works including Brenner, Tersoff, REBO, COMPASS and Morse potentials.

Modeling

In contrast to the common techniques used in mechanical engineering which are based on continuum mechanics, in MD the material is modeled as it is in fact, i.e. as a number of particles (atoms or molecules). Since in nanostructures the empty space between the particles is not negligible due to the small size, one cannot consider the medium to be continuous and thus continuum mechanics does not hold. Conversely since MD works with distinct and discrete particles, it inherently takes the discontinuity of material into account and is thus very suitable for modeling nanostructures.

The particles interact with each other. The interactions are divided into two groups: bonded and nonbonded [45]. Bonded interactions, which represent the behavior of particles having covalent bonds toward each other, are in turn categorized into bonds, angles, dihedrals and impropers. Bonds represent the tensile or compressive behavior between two atoms, angles represent the bending behavior between three atoms, dihedrals represent the torsional behavior between four linearly bonded atoms and impropers represent the torsional behavior between four centrally bonded atoms. Nonbonded interactions, which represent the behavior of particles lacking covalent bonds toward each other, are also in turn categorized into several types including van der Waals forces, electrostatic (Coulomb) effects, hydrogen bonds, many-body interactions such as the force acted upon a metallic atom (in the model of positive metallic ions in a sea of free electrons for metals) etc., each of which shows a phenomenon occurring between nonbonded atoms. Fig. 1 schematically illustrates bonded (a-d) and common nonbonded (e-f) interactions.

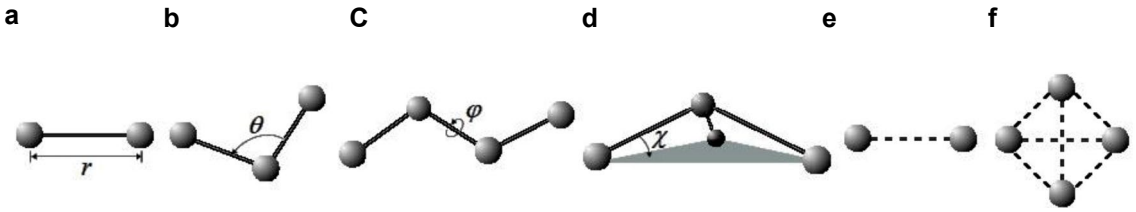

Fig. 1. Some of the interactions used in MD including bonded interactions (a) bond (b) angle (c) dihedral and (d) improper along with nonbonded interactions (e) van der Waals force and (f) many-body interaction.

In order to implement these interactions, several MATLAB codes were developed. The codes first generated the coordinates of the carbon atoms. Then 2-atom groups were distinguished for which a bond should be considered between the atoms. Similarly, 3-atom groups were identified for which an angle must be taken into account. In a similar way, 4-atom groups were recognized for which a dihedral or an improper has to be provided. A number of small but influential points were identified and followed in the codes in order to correctly find all bonds, angles, dihedrals and impropers while rejecting repeated interactions. Since in SWCNTs we only deal with carbon atoms, we have electric charge symmetry, hence no electrostatic interaction need be considered. Also, as van der Waals forces are very much weaker than bonded interactions, no such interaction was modeled [27].

Simulation

Here, we used the well-known MD package LAMMPS (Large-scale Atomic/Molecular Massively Parallel Simulator) to carry out the simulations. It is an open-source code for classical MD offering great advantages such as spatial decomposition of the simulation domain, parallel processing, easy modification or extension, and enhancement with graphics processing units [46]. Recently, it has been used to study the mechanical properties of various nanostructures [47-49]. However, similar to other MD software, it lacks graphical user interface and hence no image, video or diagram output can be directly obtained. Therefore, the codes AtomEye and ImageJ were additionally utilized to generate snapshots and simulation clips from the LAMMPS output files. Also, the output of MATLAB codes were first imported into EXCEL in order to be formatted in the form of LAMMPS commands and were then used in the input scripts. The force field functions and parameters used for the interatomic interactions are listed in Tab. 1 [26,28,50,51].

Three different methods were utilized to run the simulations as explained below: constant strain, force-constraint and constant stress.

Constant Strain Method

In the first method, which we refer to as constant strain method, the SWCNT is subjected to a desired strain and the resulting stress is read from the simulation results, and then the elastic constants are found via the relationship between strain and stress. Let us briefly review some relations from the theory of linear elasticity required for our discussion. The stiffness tensor is a fourth rank tensor relating the second rank tensors of stress and strain through the equation

$$\sigma_{ij} = c_{ijkl}\varepsilon_{kl} \tag{1}$$

Table 1. Potential functions used in MD simulations

Potential Type	Function	Parameters
Harmonic Bond	$E_r = K_r (r - r_0)^2$	K_r =20.3378 eV/Å^2 r_0 =1.42 Å
Harmonic Angle	$E_\theta = K_\theta (\theta - \theta_0)^2$	K_θ =2.73194 eV/rad^2 θ_0 =120°
2-Fold Dihedral	$E_\varphi = K_\varphi (1 - \cos(2\varphi))$	K_φ =0.157195 eV
2-Fold Improper	$E_\chi = K_\chi (1 - \cos(2\chi))$	K_χ =0.0477005 eV

Using Voigt notation [52] it can be represented by a 6×6 symmetric matrix as

$$\sigma=\begin{bmatrix}\sigma_1\\ \sigma_2\\ \sigma_3\\ \sigma_4\\ \sigma_5\\ \sigma_6\end{bmatrix}=\begin{bmatrix}\sigma_{xx}\\ \sigma_{yy}\\ \sigma_{zz}\\ \sigma_{yz}\\ \sigma_{xz}\\ \sigma_{xy}\end{bmatrix}\quad \varepsilon=\begin{bmatrix}\varepsilon_1\\ \varepsilon_2\\ \varepsilon_3\\ \varepsilon_4\\ \varepsilon_5\\ \varepsilon_6\end{bmatrix}=\begin{bmatrix}\varepsilon_{xx}\\ \varepsilon_{yy}\\ \varepsilon_{zz}\\ 2\varepsilon_{yz}\\ 2\varepsilon_{xz}\\ 2\varepsilon_{xy}\end{bmatrix}\quad C=\begin{bmatrix}C_{11} & C_{12} & C_{13} & C_{14} & C_{15} & C_{16}\\ & C_{22} & C_{23} & C_{24} & C_{25} & C_{26}\\ & & C_{33} & C_{34} & C_{35} & C_{36}\\ & & & C_{44} & C_{45} & C_{46}\\ & Sym. & & & C_{55} & C_{56}\\ & & & & & C_{66}\end{bmatrix}\quad \sigma_i=C_{ij}\varepsilon_j \tag{2}$$

which yields

$$C_{ij}=\frac{\partial\sigma_i}{\partial\varepsilon_j}=\frac{\sigma_i}{\varepsilon_j} \tag{3}$$

In writing the second equality it has been noted that C_{ij} is constant, only one strain is allowed to change at a time and the initial stress and strain tensors are assumed to be zero. Eq. (3) is used to compute the elastic constants. To do so, the SWCNT is subjected to a constant strain in a direction while other strains are kept zero, then the resulting six components of the stress tensor are obtained from the MD simulation and ultimately putting them in Eq. (3), six elements of the stiffness matrix are derived. By repeating the same procedure, each time with a different direction for strain, the whole stiffness matrix is gained.

On the other hand, SWCNT is axisymmetric and thus possesses transverse isotropy. For such a material there exist only five independent elastic constants and the stiffness matrix reduces to

$$C=\begin{bmatrix}C_{11} & C_{12} & C_{13} & 0 & 0 & 0\\ & C_{11} & C_{13} & 0 & 0 & 0\\ & & C_{33} & 0 & 0 & 0\\ & & & C_{44} & 0 & 0\\ & Sym. & & & C_{44} & 0\\ & & & & & (C_{11}-C_{12})/2\end{bmatrix} \tag{4}$$

In addition to the elastic constants, we may find the Young's and shear moduli as well as Poisson's ratios by calculating the compliance tensor and using the following equation

$$S=C^{-1}=\begin{bmatrix}1/E_x & -\nu_{yx}/E_x & -\nu_{zx}/E_z & 0 & 0 & 0\\ & 1/E_x & -\nu_{zx}/E_z & 0 & 0 & 0\\ & & 1/E_z & 0 & 0 & 0\\ & & & 1/G_{xz} & 0 & 0\\ & Sym. & & & 1/G_{xz} & 0\\ & & & & & 1/G_{xy}\end{bmatrix} \tag{5}$$

Force-Constraint Method

In the second method, which we call force-constraint method, the SWCNT is treated much like a macroscopic structure. The atoms placed on one end of the SWCNT are constrained such that they are not allowed to move, and the atoms on the other end are subjected to individual forces. The simulation is run until all atoms reach their equilibrium positions. Using the results of the simulation, the deformation of the SWCNT is calculated. Next, considering an equivalent continuum tube with a wall thickness equal to the van der Waals diameter of carbon, that is 3.4 Å [1,3,8,11,26,30,31,33], and applying the following relations from elasticity, Young's and shear moduli are derived. Young's modulus is found via

$$E=\frac{FL}{A\overline{\Delta}} \tag{6}$$

where F is the total axial force exerted on the end atoms, L is the initial length of SWCNT, A is its equivalent cross sectional area calculated as $2\pi rt$ where r is its radius and t=3.4 Å, and finally $\overline{\Delta}$ is the average calculated axial deformation. Similarly, shear modulus is determined through

$$G=\frac{TL}{J\overline{\varphi}} \tag{7}$$

where T is the total torque applied by exerting circumferential forces on the end atoms, J is the polar moment of inertia of the equivalent cross sectional area of SWCNT calculated as $2\pi rt(r^2+t^2/4)$ and $\overline{\varphi}$ is the average calculated torsional deformation.

Constant Stress Method

In the third method, which is referred to as constant stress method, the SWCNT is subjected to a specified stress and the consequent deformation is obtained from the simulation. In case of Young's modulus, axial stress is applied and the equation

$$E=\frac{\sigma}{\varepsilon}=\frac{\sigma}{\overline{\Delta}/L} \tag{8}$$

is used where σ is the applied axial normal stress, while in case of shear modulus, torsional shear stress is applied and the equation

$$G = \frac{\tau}{\gamma} = \frac{\tau}{r\bar{\varphi}/L} \tag{9}$$

is used in which τ is the applied torsional shear stress.

RESULT

The simulations were carried out on armchair SWCNTs with chirality indices of (4,4), (6,6), (8,8), (10,10), (12,12) and (14,14) all having an initial length of 100.840 Å and zigzag SWCNTs with chirality indices of (8,0), (12,0), (16,0), (20,0), (24,0) and (28,0) all having an initial length of 100.820 Å at zero temperature. The smallest model is (4,4) possessing 664 atoms, 988 bonds, 1960 angles, 3896 dihedrals and 648 impropers while the biggest one is (28,0) possessing 2688 atoms, 4004 bonds, 7952 angles, 15792 dihedrals and 2632 impropers. The axis of the SWCNTs was coincided with the z-axis of the coordinate system. The (8,8) SWCNT model is shown in Fig. 2 as an example.

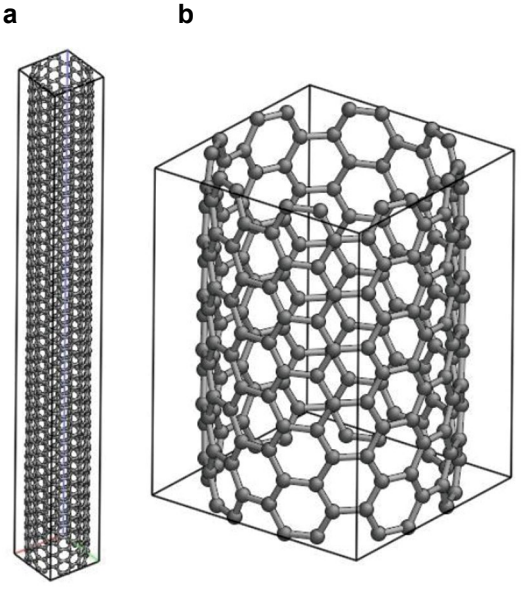

Fig. 2. A snapshot of a typical simulated SWCNT produced by LAMMPS and AtomEye (a) full view (b) partial view.

The information of SWCNT topology for each model along with its defined interatomic interactions and simulation box properties were placed in a data file which was invoked by the input script of LAMMPS commands. Since the elastic properties have a static nature, the simulations were performed at zero temperature. The algorithm utilized in energy minimizations was the Polak-Ribiere version of the conjugate gradient algorithm. Fixed boundary conditions were applied. The simulations were run on an Intel Core 2 Duo CPU with 2 GB RAM on 64-bit Windows 8 platform. Output files were dumped from LAMMPS at regular intervals during the simulations to provide the data required for calculations and visualizations carried out by AtomEye and ImageJ. All models were first relaxed to insure the condition of zero initial stress and strain. Then the elastic constants and moduli were computed via the three methods. In order to get better results, in constant strain method both positive and negative strains were simulated and in the other two methods both tensile and compressive forces and stresses were applied. Then the results were averaged.

As typical examples, using strains equal to ±0.1, constant strain method resulted in the following elastic constants for the (8,8) and (16,0) SWCNTs

$$\begin{aligned}&(8,8):\ C_{11}=351\ \ C_{12}=117\ \ C_{13}=83\ \ C_{33}=930\ \ C_{44}=194\ \ C_{66}=118\ \ \text{GPa}\\&(16,0):\ C_{11}=353\ \ C_{12}=118\ \ C_{13}=84\ \ C_{33}=927\ \ C_{44}=196\ \ C_{66}=119\ \ \text{GPa}\end{aligned}$$

which in turn give the following moduli and Poisson's ratios.

$$\begin{aligned}&(8,8):\ E_x=309\ \ E_z=901\ \ G_{xz}=194\ \ G_{xy}=118\ \ \text{GPa}\ \ \nu_{zx}=0.177\ \ \nu_{yx}=0.319\\&(16,0):\ E_x=310\ \ E_z=897\ \ G_{xz}=196\ \ G_{xy}=119\ \ \text{GPa}\ \ \nu_{zx}=0.178\ \ \nu_{yx}=0.320\end{aligned}$$

Note that in both cases, $(C_{11}\text{-}C_{12})/2 \approx C_{66}$ which verifies the transverse isotropy of SWCNT. Since the elastic constants obtained for the other models are very close to the above values, and also to enable comparison with the other methods we continue with Young's and shear moduli. The results of constant strain method may be summarized as in Fig. 3. The magnitude of the applied strain in these simulations was 0.1.

Similarly, the results of force-constraint method are presented in Fig. 4. The applied force per end atom in these simulations was 1 eV/Å. Finally, the results of constant stress method are depicted in Fig. 5. In the associated simulations, the constant applied stress for each SWCNT was dependent on its size, ranging between 18.7-21.8 GPa for axial normal stress and 9.1-18.9 GPa for torsional shear stress.

As we have used anharmonic nonlinear interatomic potentials, one may be interested to study the effect of this nonlinearity on the results. Thus in each method the loading conditions, i.e. the strain in constant strain method, the applied force per end atom in force-constraint method and the stress in constant stress method, were altered. The attained results for the typical (8,8) SWCNT are shown in Fig. 6.

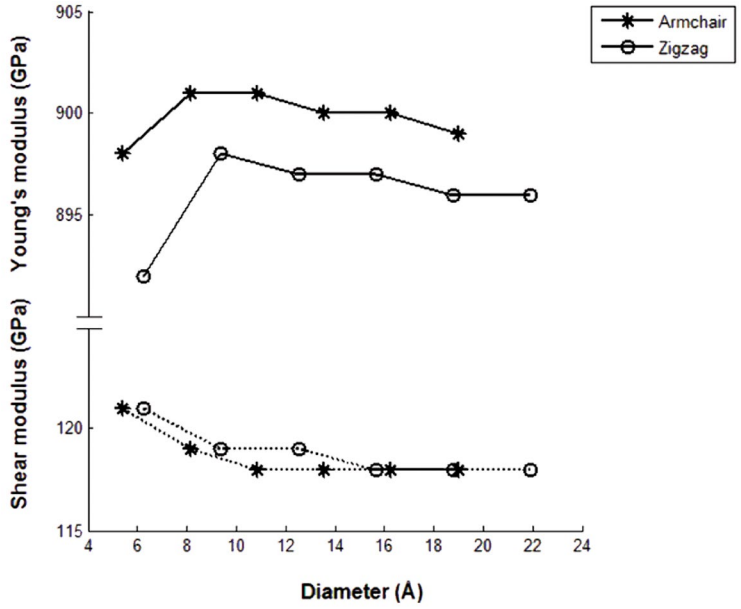

Fig. 3. Results of constant strain method.

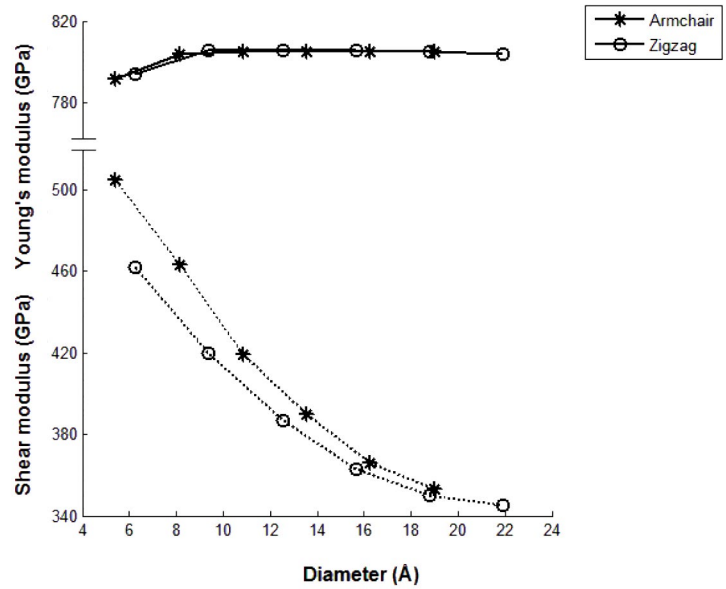

Fig. 4. Results of force-constraint method.

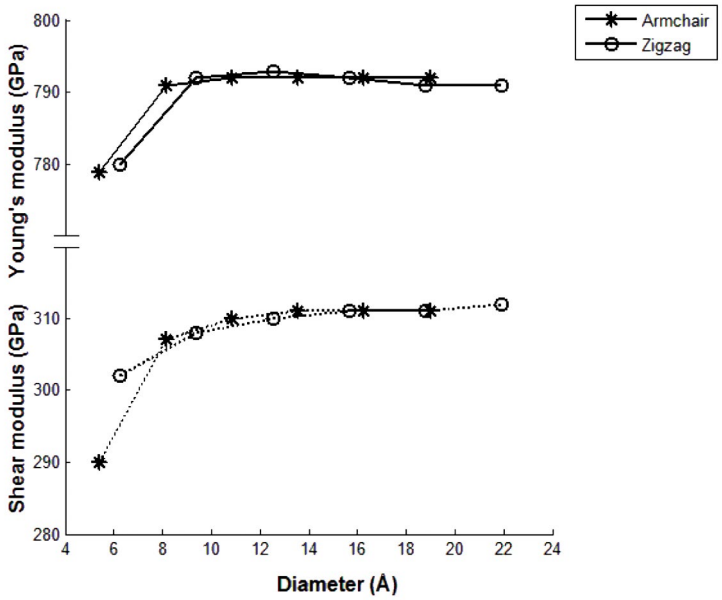

Fig. 5. Results of constant stress method.

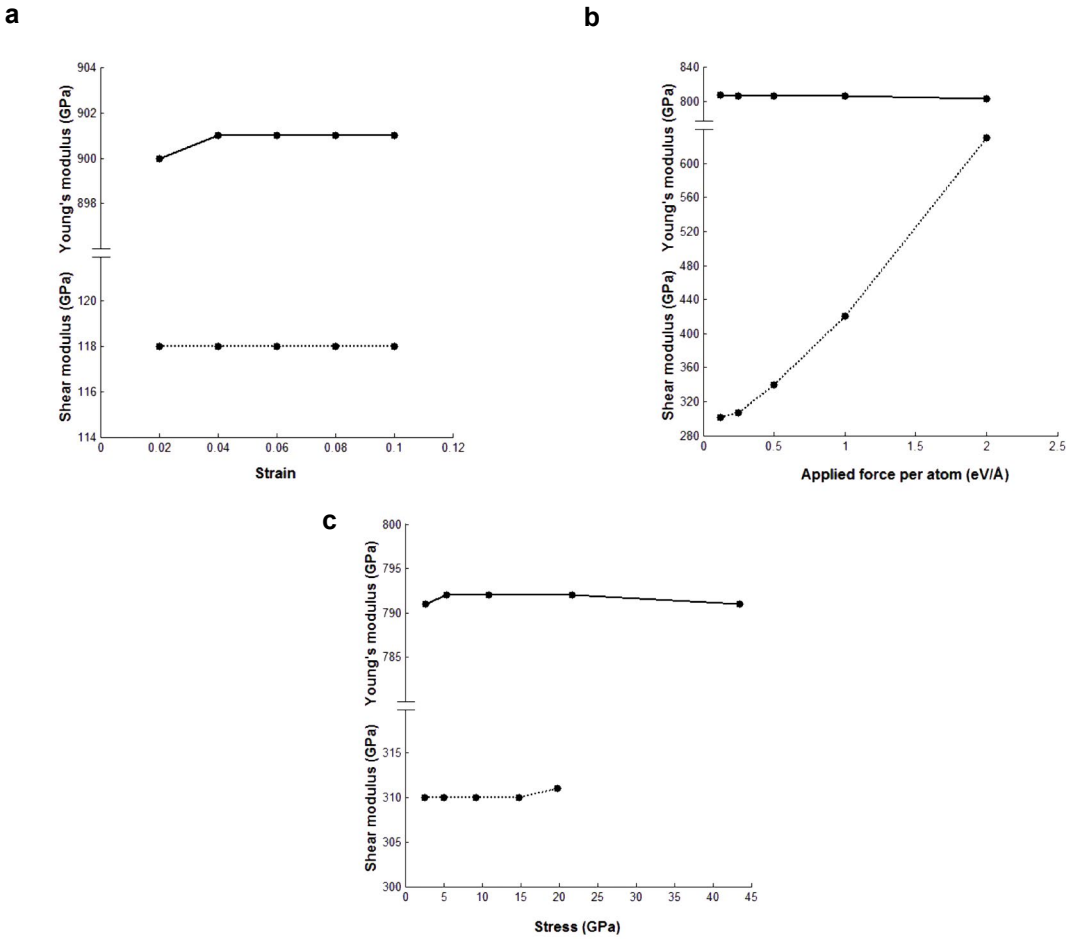

Fig. 6. Effect of loading conditions on the moduli in (a) constant strain method (b) force-constraint method and (c) constant stress method.

DISCUSSION

Looking back at Fig. 3 for constant strain method, we may deduce that for a typical SWCNT Young's modulus is around 900 GPa and shear modulus is about 120 GPa. Although the moduli change with chirality and diameter, the changes are small. Compared to the literature, the attained value of 900 GPa is satisfactorily close to the well-known Young's modulus of around 1 TPa but the obtained shear modulus of 120 GPa is nearly 70% far from the expected value of about 400 GPa. It is also smaller than the minimum reported value of 240 GPa. The reason behind that seems to be the different conditions of loading and deformation of the SWCNT. Usually, shear modulus is found by loading the SWCNT under torsion, but the method used here forces us to apply pure shear. In the former the cross section tends to remain close to a circle but in the latter it tends to become close to an ellipse. Clearly, the way that bonds, angles, dihedrals and impropers undergo changes are completely different in the two conditions. In torsion nearly all of the interactions are involved, resulting in a greater resistance against the load and thus a higher modulus. In shear, however, a limited percent of the interactions really feel the load, hence the deformation is more, resulting in a lower modulus. It seems that torsional loading is more reasonable because in practice pure shear is not likely but torsion is a very natural load. In fact, pure shear is of theoretical significance only but what we really deal with is torsion. Thus, in the second and third methods torsion was used.

Fig. 4 for force-constraint method suggests that Young's modulus is nearly 800 GPa but shear modulus highly decreases by increasing the diameter. Chirality is not as influential as diameter. The value of 800 GPa is acceptable according to the literature. As mentioned above in this method, as well as the third method, torsion is used to derive the shear modulus. Therefore, although the values of shear modulus decrease by diameter but they are still much higher than those of constant strain method. These values are distributed well around the approximate expectation of 400 GPa. The authors believe that the high dependence of shear modulus on diameter goes back to the attribution of an assumptive wall thickness and hence cross sectional area to the SWCNT. The polar moment of inertia of this area which appears in the denominator of Eq. (7) is proportional to r3 while the torque appearing in the numerator is proportional to r^2. Thus the shear modulus decreases due to increase in diameter. It is noteworthy that Eq. (6) does not suffer from such a problem because both the area in the denominator and the total force in the numerator are proportional to r. Based on this argument, one can conclude that since force-constraint method involves assumption of an equivalent wall thickness, care must be taken to avoid its artifacts.

One can observe in Fig. 5 for constant stress method that a Young's modulus of approximately 790 GPa is predicted which is a good outcome as the 800 GPa of the previous method. Also a value of about 310 GPa is derived for shear modulus. As can be seen, the effect of chirality and diameter is negligible. The obtained shear modulus of 310 GPa is again much greater than that of constant strain method. Also it is admissible compared to the average value of 400 GPa of the literature. The main difference between this third method and the second method is that here no wall thickness is assumed. That is, in force-constraint method we compute the stress by manipulating the applied force and the equivalent cross sectional area, but in constant stress method we directly work with stress. In other words, constant stress method can be interpreted as a modified force-constraint method. This is why their results are close while the shear modulus of constant stress method does not suffer from the severe diameter dependence of force-constraint method.

Fig. 6 implies that generally the nonlinearity due to anharmonic potentials is not remarkable in all three methods, since changing the loading conditions does not alter the results significantly. This is mainly due to the weakness of nonlinear dihedral and improper terms compared to the linear bond and angle terms (derivatives of the potential functions) according to the parameters listed in Tab. 1. One exception in this figure is the shear modulus in force-constraint method which has large variations with respect to the applied force. But as discussed above, this is an artifact of assuming wall thickness and cross sectional area for SWCNT in such a way that the calculated torsional shear stress using the polar moment of inertia of the area becomes unboundedly large for large forces, resulting in high shear moduli. Therefore this is not an exception in fact and the results of the modified method, i.e. constant stress method, should be considered instead, which are calculated using the correct shear stress.

CONCLUSION

Elastic constants, Young's and shear moduli, and Poisson's ratios of armchair and zigzag SWCNTs were derived through MD simulations via three methods: constant strain, force-constraint and constant stress. Broad ranges were obtained and their accuracy was discussed. Overall, based on the results and discussions one can conclude that values of 790-900 GPa for Young's modulus and 310-400 GPa for shear modulus of typical SWCNTs were obtained. These concluding values well agree with the expected values anticipated from the data reported in the literature, obtained via various theoretical or experimental techniques.

However, the applied methods also resulted in some unacceptable or incorrect results recognized by comparison with either each other or the literature. In particular, constant strain method works well for the determination of normal elastic constants and Young's modulus but is not as good in the prediction of shear elastic constants and shear modulus. Anyway, it can be a powerful tool as far as the elastic constants are concerned rather than the elastic moduli. Force-constraint method is easy to understand and implement but may come with serious artifacts which need care when dealing with. Being a modified force-constraint method, constant stress method seems to be more reliable. It also results in conservative lower bound values.

Generally the structural details of SWCNT, namely chirality and diameter, do not affect its elastic properties significantly. The same statement is true for the nonlinearity of dihedral and improper interactions.

ACKNOWLEDGMENT

The authors are very grateful to the Iran Nanotechnology Initiative Council for its financial and intellectual support of this work.

CONFLICT OF INTEREST

The authors declare that there is no conflict of interests regarding the publication of this manuscript.

REFERENCES

1. D. Qian, G.J. Wagner, W.K. Liu, M.F. Yu and R.S. Ruoff, Appl. Mech. Rev., 55(6), 495 (2002).
2. E.T. Thostenson, Z. Ren and T.W. Chou, Compos. Sci. Technol., 61(13), 1899 (2001).
3. M.F. Yu, J. Eng. Mater. T. ASME, 126(3), 271 (2004).
4. D. Srivastava, C. Wei and K. Cho, Appl. Mech. Rev., 56(2), 215 (2003).
5. A. Kis and A. Zettl, Philos. T. Roy. Soc. A, 366(1870), 1591 (2008).
6. L.C. Zhang, J. Mater. Process. Tech., 209(9), 4223 (2009).
7. E.T. Thostenson, C. Li and T.W. Chou, Compos. Sci. Technol., 65(3), 491 (2005).
8. R.S. Ruoff, D. Qian and W.K. Liu, C. R. Phys., 4(9), 993 (2003).
9. A. Maiti, Microelectron. J., 39(2), 208 (2008).
10. F. Li, H.M. Cheng, S. Bai, G. Su and M.S. Dresselhaus, Appl. Phys. Lett., 77(20), 3161 (2000).
11. A. Sears and R.C. Batra, Phys. Rev. B, 69(23), 235406 (2004).
12. J.P. Lu, Phys. Rev. Lett., 79(7), 1297 (1997).
13. H.C. Cheng, Y.L. Liu, Y.C. Hsu and W.H. Chen, Int. J. Solids Struct., 46(7), 1695 (2009).
14. S.C. Chowdhury, B.Z.G. Haque, J.W. Gillespie and D.R. Hartman, Comp. Mater. Sci., 65, 133 (2012).
15. M. Rossi and M. Meo, Compos. Sci. Technol., 69(9), 1394 (2009).
16. J. Geng and T. Chang, Phys. Rev. B, 74(24), 245428 (2006).
17. C.L. Zhang and H.S. Shen, Appl. Phys. Lett., 89(8), 081904 (2006).
18. A.R. Hall, L. An, J. Liu, L. Vicci, M.R. Falvo, R. Superfine and S. Washburn, Phys. Rev. Lett., 96(25), 256102 (2006).
19. A.R. Khoei, E. Ban, P. Banihashemi and M.A. Qomi, Mater. Sci. Eng. C, 31(2), 452 (2011).
20. Y.Y. Zhang, C.M. Wang and Y. Xiang, Carbon, 48(14), 4100 (2010).
21. M.M. Zaeri, S. Ziaei-Rad, A. Vahedi and F. Karimzadeh, Carbon, 48(13), 3916 (2010).
22. C.H. Wong, Comp. Mater. Sci., 49(1), 143 (2010).
23. B. WenXing, Z. ChangChun and C. WanZhao, Physica B, 352(1), 156 (2004).
24. H. Xin, Q. Han and X.H. Yao, Carbon, 45(13), 2486 (2007).
25. J.Y. Hsieh, J.M. Lu, M.Y. Huang and C.C. Hwang, Nanotechnology, 17(15), 3920 (2006).
26. C. Li and T.W. Chou, Int. J. Solids Struct., 40(10), 2487 (2003).
27. C. Li and T.W. Chou, Compos. Sci. Technol., 63(11), 1517 (2003).
28. A.L. Kalamkarov, A.V. Georgiades, S.K. Rokkam, V.P. Veedu and M.N. Ghasemi-Nejhad, Int. J. Solids Struct., 43(22), 6832 (2006).
29. P. Zhang, Y. Huang, P.H. Geubelle, P.A. Klein and K.C. Hwang, Int. J. Solids Struct., 39(13), 3893 (2002).
30. P.M. Agrawal, B.S. Sudalayandi, L.M. Raff and R. Komanduri, Comp. Mater. Sci., 38(2), 271 (2006).
31. Q. Lu and B. Bhattacharya, Nanotechnology, 16(4), 555 (2005).
32. A. Fereidoon, M.G. Ahangari, M.D. Ganji and M. Jahanshahi, Comp. Mater. Sci., 53(1), 377 (2012).
33. X. Chen and G. Cao, Nanotechnology, 17(4), 1004 (2006).
34. T. Chang and H. Gao, J. Mech. Phys. Solids, 51(6), 1059 (2003).
35. Z. Yao, C.C. Zhu, M. Cheng and J. Liu, Comp. Mater. Sci., 22(3), 180 (2001).
36. Y.I. Prylutskyy, S.S. Durov, O.V. Ogloblya, E.V. Buzaneva

and P. Scharff, Comp. Mater. Sci., 17(2), 352 (2000).

37. Y. Jin and F.G. Yuan, Compos. Sci. Technol., 63(11), 1507 (2003).
38. K.M. Liew, X.Q. He and C.H. Wong, Acta Mater., 52(9), 2521 (2004).
39. Y. Wang, X.X. Wang, X.G. Ni and H.A. Wu, Comp. Mater. Sci., 32(2), 141 (2005).
40. Z. Wang, M. Devel and B. Dulmet, Surf. Sci., 604(5), 496 (2010).
41. K. Mylvaganam and L.C. Zhang, Carbon, 42(10), 2025 (2004).
42. B. Motevalli, A. Montazeri, R. Tavakoli-Darestani and H. Rafii-Tabar, Physica E, 46, 139 (2012).
43. X. Hao, H. Qiang and Y. Xiaohu, Compos. Sci. Technol., 68(7), 1809 (2008).
44. W.H. Duan, Q. Wang, K.M. Liew and X.Q. He, Carbon, 45(9), 1769 (2007).
45. E.B. Tadmor and R.E. Miller, "Modeling materials: continuum, atomistic and multiscale techniques", Cambridge University Press, 259 (2011).
46. S. Plimpton, J. Comput. Phys., 117(1), 1 (1995).
47. F. Memarian, A. Fereidoon, S. Khodaei, A.H. Mashhadzadeh and M.D. Ganji, Vacuum, 139, 93 (2017).
48. A. Fereidoon, M. Mostafaei, M.D. Ganji and F. Memarian, Superlattice. Microst., 86, 126 (2015).
49. M.M. Zaeri and S. Ziaei-Rad, AIP Adv., 5(11), 117114 (2015).
50. W.D. Cornell, P. Cieplak, C.I. Bayly, I.R. Gould, K.M. Merz, D.M. Ferguson, D.C. Spellmeyer, T. Fox, J.W. Caldwell and P.A. Kollman, J. Am. Chem. Soc., 117(19), 5179 (1995).
51. W.L. Jorgensen and D.L. Severance, J. Am. Chem. Soc., 112(12), 4768 (1990).
52. M.H. Sadd, "Elasticity: theory, applications and numerics", 2nd ed., Academic Press, 298 (2009).